# Hydration and Dynamics in Reverse Micelles of the Triblock Copolymer $EO_{13}PO_{30}EO_{13}$ in Water/*o*-Xylene Mixtures: A Spin Probe Study

**Agneta Caragheorgheopol,[†] Jan Pilar,[‡] and Shulamith Schlick***

*Department of Chemistry, University of Detroit Mercy, Detroit, Michigan 48219, and Institute of Macromolecular Chemistry, Academy of Sciences of the Czech Republic, Heyrovsky Sq. 2, 162 06 Prague 6, Czech Republic*

*Received November 26, 1996; Revised Manuscript Received March 4, 1997*[⊗]

ABSTRACT: The reverse micellar phase $L_2$ of the triblock copolymer poly(ethylene oxide)-*b*-poly(propylene oxide)-*b*-poly(ethylene oxide) $EO_{13}PO_{30}EO_{13}$ (commercial name Pluronic L64), where EO is ethylene oxide and PO is propylene oxide, was studied in the ternary mixture L64/water/*o*-xylene and in the binary mixture L64/water, using ESR spectroscopy with nitroxide spin probes. The spin probes differed in size, structure, and polarity and belong to two main types: (a) cationic probes 4-(*N*,*N*-dimethyl-*N*-alkyl)-ammonio)-2,2′,6,6′-tetramethylpiperidine-1-oxyl iodide (CAT*n*) with *n*, the number of carbon atoms in the alkyl substituent, equal to 1, 4, 8, 11, and 16; (b) amphiphilic probes based on *x*-doxylstearic acid (*x*DSA) with *x*, the carbon atom to which the doxyl group is attached, equal to 5, 7, 10, and 16. X-band ESR spectra reflect the intercalation of the probes in the self-assembled L64 system, but different probes choose different locations in the aggregates and report on the *local* polarity, hydration, and degree of order. The hydration gradient in the poly(ethylene oxide) (PEO) core of the reverse micelles was estimated on a scale of ≤48 Å from the analysis of $a_N$, the isotropic hyperfine splitting of $^{14}N$, in the CAT*n* series by comparison with a "calibration curve" based on CAT4 in aqueous solutions of PEO. The lower homologs in the series ($n = 1$ and 4) are located near the center of the hydrated core, while the higher homologs ($n = 11$ and 16) are close to the interface between the hydrated core and the *o*-xylene-swollen poly(propylene oxide) (PPO) blocks. The *x*DSA probes have their head group near the interface between the core and the PPO regions. The nitroxide group in 5DSA is at the core/PPO interface, but the nitroxide groups in the other doxyl probes are at different depths in the PPO regions, depending on the value of *x*. The dynamics of the CAT*n* probes was elucidated by comparing the experimental *B* and *C* parameters in the expression for the line width in motionally averaged ESR spectra of nitroxides $\Delta H(m_I) = A + Bm_I + Cm_I^2$, with the corresponding values calculated as a function of the direction of the axis of rotation and *N*, the degree of anisotropy of the rotational reorientation. The comparison suggests that the dominant motional mechanism for all probes is rotation around the N−O bond (*x* axis), but the anisotropy of the lower spin probe homologs is significantly higher ($N = 10$) compared to that of the higher homologs ($N = 2-3$). These results are consistent with the existence of a hydration gradient in the core of the reverse micelles.

## Introduction

Reverse micelles (RM) formed by ionic surfactants in a mixture of water and a hydrocarbon as the "oil" have been extensively studied in recent years because they provide easily controlled model compounds for the behavior of biomembranes and could improve our understanding of reactivities and interactions in confined media.[1,2] Bis(2-ethyl-1-hexyl) sulfosuccinate (AOT) is the best known representative of this class of compounds and has been studied by numerous methods.[1−4] Electron spin resonance (ESR) spectroscopy based on nitroxide spin probes[3,5] and paramagnetic transition metal cations[4] has provided local information on the nature of water in the "water pools" (bulk vs. bound), the polarity of the aggregates, and the connectivity of the water pools.

Reverse micelles of nonionic alkyl− and alkyl−aryl-oligo(ethylene oxide) have been studied more recently, and as a result of ≈10 years of experimental and theoretical studies, a general picture of self-assembling has emerged.[6−11] Water plays a crucial role in the micellization process and determines the size and structure of the aggregates: no significant association has been detected in the absence of water. The aggregation number usually increases with the water content, and at higher water contents a water-rich core is formed, where the water properties are modified by the interaction with the surfactant and differ from those of pure water. Spin probes and fluorescent probes have been used in a study of reverse micelles of poly(ethylene oxide) alkyl ethers, with cyclohexane or decane as the oil.[12,13] The $^{14}N$ isotropic hyperfine splitting, $a_N$, of the nitroxide group in a small cationic spin probe has been the quantity used to monitor the polarity of the probe site and to provide an *effective* hydration number, $Z_{w,eff}$, in water molecules per ethylene oxide (EO) group. $Z_{w,eff}$ has been compared with the *average* hydration number $Z_w$ calculated from the *total* number of water molecules and EO units. For calibration, $a_N$ has been measured as a function of the water content in solutions of poly(ethylene oxide) (PEO), a system where aggregation is not expected. The ionic spin probe has revealed the existence of regions with higher than average water content; a fluorescent probe, 1-anilinonaphthalene-8-sulfonic acid, has reported on regions with lower than average hydration.

The nonionic water-soluble polymeric surfactants that consist of poly(ethylene oxide) (PEO) and poly(propylene oxide) (PPO) segments, Chart 1, are commercially

* To whom all correspondence should be addressed at the University of Detroit Mercy. E-mail address: SCHLICKS@UDMERCY.EDU.

[†] University of Detroit Mercy, on leave from the Institute of Physical Chemistry, Romanian Academy of Sciences, Bucharest, Romania.

[‡] Institute of Macromolecular Chemistry.

[⊗] Abstract published in *Advance ACS Abstracts,* April 15, 1997.

S0024-9297(96)01732-9 CCC: $14.00 

**Chart 1. PEO−PPO−PEO Triblock Copolymers**

$$HO[-CH_2CH_2O-]_m[-CH(CH_3)CH_2O-]_n[-CH_2CH_2O-]_mH$$

$$(EO_mPO_nEO_m)$$

available as triblocks PEO−PPO−PEO in a range of molecular masses and ratios of the two components and are used in diverse applications such as detergents, stabilizers, emulsifiers, cosmetics, drug release, treatment of burns, and water purification.[14,15] The copolymers, made by BASF ("Pluronics") and ICI ("Poloxamers"), can also be obtained with the EO block in the center and the propylene oxide (PO) block on the outside ("reverse Pluronics"), or in a dendrimer architecture with PEO−PPO or PPO−PEO chains linked to an ethylenediamine core.[16]

The most characteristic property of the Pluronic diols is the *inverse* temperature dependence of the critical micelle concentration (cmc): the cmc decreases as the temperature increases.[14,15] Interesting rheological properties follow, and gel phases are formed in some Pluronics with increase in temperature, due to the growth of the micelles and the interpenetration of their coronas. This behavior has been successfully modeled by Karlstrom *et al.*,[17] Linse,[18] and Hurter *et al.*,[19] based on the analysis of the chain conformations expected for polymers containing the $-CH_2CH_2O-$ group: trans and gauche sequences lead to polar or nonpolar conformers, and the number of the nonpolar conformers increases with temperature, leading to less favorable interactions with water and "shrinkage" of the exterior of PEO block exposed to water. As expected intuitively, calculations show that the micelle interior is primarily composed of PO units, and the corona is primarily EO units. Phase diagrams predicted by this approach are in reasonable agreement with the experiment, especially for Pluronics with a relatively simple phase diagram that consists of spherical and elongated micelles at low temperatures and phase separation at higher temperatures.[19] The Pluronics have been investigated by theoretical methods and by a variety of experimental methods including viscometry, light scattering, nuclear magnetic resonance (NMR), UV−vis of selected probes, surface tension, and fluorescence.[14−20]

The Pluronic block copolymers have the same hydrophilic part (PEO) as the nonionic surfactants mentioned above; the difference in polarity between the hydrophilic PEO and the hydrophobic PPO blocks is, however, less pronounced than that between the "head group" (PEO) and "tail" (usually hydrocarbon) in the nonionic surfactants. Therefore, the question of a selective solvent is more delicate.

For the formation of reverse micelles, the requirement is that the volume of the PPO block with its solvation sphere be greater than the volume of the PEO block solvated by water.[21] Chu and co-workers have reported on the reverse micellar phase in $EO_{13}PO_{30}EO_{13}$ (Pluronic L64) in a mixture of *o*-xylene/water.[22,23] L64 is miscible in *o*-xylene in all proportions. Evidence for the formation of RM has been found only in the presence of water: micelles with a hydrated PEO core and a heavily solvated (by the organic solvent) PPO corona form when the number of water molecules per EO unit is >0.15. $^1$H NMR spectroscopy has indicated that the chemical environment of the protons in the methyl and −CH< groups of PPO is unchanged for water content up to $Z_w = 2.61$, suggesting no water penetration into the nonpolar regions.[22] Small angle neutron scattering (SANS) experiments have shown that some water is solubilized in the corona, but the amount is ≈40 times lower than that in the PEO domains.[23]

**Chart 2. Spin Probes Used in This Study**

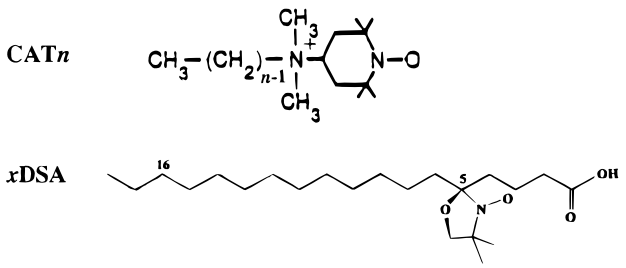


The phase diagram at 298 K of the system L64/water/*p*-xylene has been recently determined[24] using polarizing microscopy and measurement of the quadrupolar splitting of $^2$H by NMR, and the extent of the $L_2$ phase has been defined; *p*-xylene has been chosen because the symmetry of the methyl groups facilitates the interpretation of $^2$H NMR spectra. Experiments with both xylene isomers have indicated that *o*- and *p*-xylene give identical phase diagrams in the ternary system. The authors have also mentioned that use of $^2H_2O$ (instead of $^1H_2O$) facilitates phase separation because of the higher density of $^2H_2O$ and leads to minor changes only in the phase diagram.[24] To the best of our knowledge, no other studies on the $L_2$ phase in any Pluronics have been reported.

We have initiated a study of Pluronics using spin probe ESR spectroscopy as a source of structural and dynamical data, ESR imaging (ESRI) for the determination of the translational diffusion coefficients of various spin probes, and viscosity measurements for comparison of microscopic and macroscopic data. Preliminary results on the binary L64/water system as a function of L64 content based on amphiphilic probes, with focus on the lamellar phase,[25] and an ESR and ESRI study of L64/water based on a nonionic hydrophilic probe[26] have been published.

We present a study of the $L_2$ phase in $EO_{13}PO_{30}EO_{13}$ using a series of cationic and amphiphilic spin probes, CAT*n* and *x*-doxyl stearic acid (*x*DSA) spin probes, respectively (Chart 2). The main objective of this study is to determine the local polarities in the L64 reverse micelles for different water contents, with emphasis on the polar core. The identical nitroxide moiety in the CAT*n* spin probes ensures that any changes in the line shapes and magnetic parameters are due to variations in the probe environment. The *x*DSA probes, however, are only slightly soluble in water, and are expected to be solubilized in, and to report on, the less polar and less hydrated regions.[27−29]

## Experimental Section

**Materials.** The Pluronic L64 block copolymer, with a molecular weight (MW) of 2900 and ≈40% w/w PEO, was a gift from BASF Corp. and was used as received; the corresponding formula is $EO_{13}PO_{30}EO_{13}$. The number-average MW $M_n$ (3400 g/mol, determined by vapor pressure osmometry), together with the weight-average MW $M_w$ (3700 g/mol, from light scattering) indicate a low polydispersity ratio, $M_w/M_n = 1.1$.[22] The water content determined by the Karl Fisher method, 0.35% w/w, corresponds to $Z_w = 0.02$, where $Z_w$ is the number of water molecules per EO unit; this value was taken into consideration when preparing the aqueous solutions of L64. Anhydrous *o*-xylene (Aldrich, 97% pure) was shipped and kept under nitrogen. PEO (Carbowax 300 from Union Carbide), PPO (MW 2000, from Aldrich), and tetraethyleneglycol

**Chart 3. The "quencher" $CuX_2$, Where X = 1-Methyl-2-carbethoxyglyoxal 1-(*p*-Tolylanil) 2-(*m*-Tolylhydrazone)**

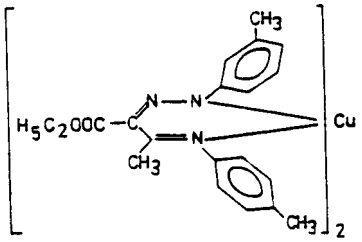

dimethyl ether (TEDGME, from Aldrich) were used without further purification.

Two types of nitroxide spin probes were used in this study (Scheme 2): (a) the cationic spin probes 4-(*N*,*N*′-dimethyl-*N*-alkylammonio)-2,2′,6,6′-tetramethylpiperidine-1-oxyl iodide (CAT*n*) with *n*, the number of carbon atoms in the alkyl substituent equal to 1, 4, 8, 11, and 16, were from Molecular Probes, Eugene, OR; (b) the *x*-doxyl stearic acid probes (*x*DSA) with *x*, the carbon atom to which the doxyl group is attached, equal to 5, 7, 10, 12, and 16, were from Sigma Chemical Co. All spin probes were used as received.

**Sample Preparation.** The solution of L64 in *o*-xylene (0.316 g/mL solution, corresponding to 34.5% w/w solvent) was prepared and stored for several days before use. Specific amounts of water were added to obtain $Z_w = 0.25$, 0.50, 0.75, 1.00, and 2.00; these solutions are in the $L_2$ phase.[24] Water dissolution was immediate and the resulting transparent solutions were stable for at least six months. The binary L64/water solution (86.1% w/w copolymer), which is also in the $L_2$ phase,[24] was prepared by weighing the components and storing the solution for a few days to ensure complete mixing.

The spin probes were added to the L64 binary or ternary solutions by the following procedure: the required amount of spin probe from a stock ethanol solution (usually ≈5 mM) was divided into several vials, the solvent was evaporated in air, and a corresponding amount of the surfactant solution was added to yield a final spin probe concentration in the 0.1−0.5 mM range. The samples were stirred with a vortex for 5 min, left overnight to ensure solubilization of the probe, and sealed with parafilm to prevent evaporation of solvents.

The dissociation constant of the carboxyl group in the *x*DSA spin probes is pH dependent; in order to avoid ambiguity and to obtain reproducible results, we opted to prepare L64 solutions in 0.1 M aqueous NaOH instead of pure water. Although some changes in the phase diagram are possible, we did not detect any changes in the spectral parameters for the CAT*n* spin probes in these solutions compared to aqueous solutions; it seems that the structure of the micellar interior is little, if at all, affected by the modification of the pH. We note that, in the reverse micelles based on AOT, the spectrum of 5DSA is the same for solutions with pH values in the range 6.3−9.0.[3]

**Calibration of $a_N$.** In order to correlate the variation of $a_N$ in the L64 system to the degree of local hydration of the monomer segments, we measured the $a_N$ values of the CAT*n* probes in aqueous PEO (Carbowax 200 and 300) as a function of $Z_w$, in the temperature range 283−333 K. The expected lack of aggregation in the PEO solutions ensures that the amount of water per monomer unit represents also the effective hydration sensed by the probe. Representative $a_N$ values used for comparison with the corresponding values in L64 were chosen when a plateau of $a_N$ vs temperature was obtained, because the most accurate $a_N$ values can be measured when the anisotropy of the spectral parameters is averaged. The $a_N$ values for CAT1 and for CAT4 are constant with temperature, within experimental error. As reference in the comparison with the aggregated system, we used the ESR spectra of CAT4 in aqueous solutions of Carbowax 200 as a function of $Z_w$.[13]

**Selective Quenching.** The location of probes and the penetration of solvent into the aggregates were verified by addition of two line broadening molecules: $CuCl_2$ as the water-soluble paramagnet, and $CuX_2$ (where X = 1-methyl-2-carbethoxyglyoxal 1-(*p*-tolylanil) 2-(*m*-tolylhydrazone), Chart 3) as the oil-soluble paramagnet. In the quenching experiments, the samples containing the spin probes were treated with $CuCl_2$ or $CuX_2$ until successive additions had no effect on the spectra. Typical amounts used were ≈1 mg of $CuCl_2$/0.1 g of sample, and ≈5 mg of $CuX_2$/0.1 g of sample.

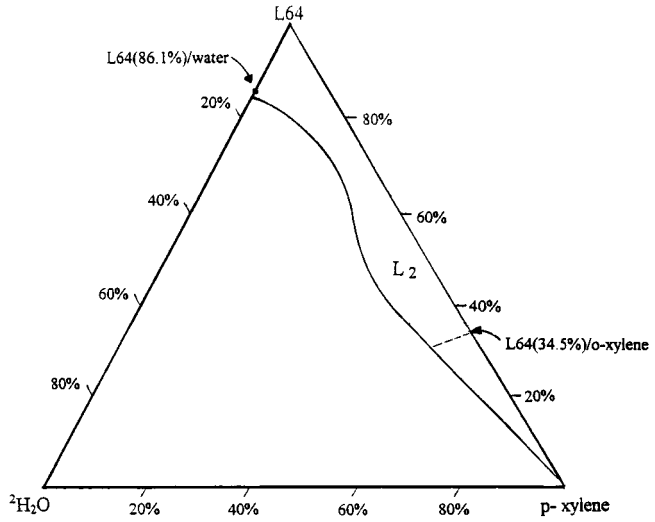


**Figure 1.** The $L_2$ portion of the phase diagram for L64/water/*p*-xylene at 298 K (redrawn).[24] The ternary compositions in the $L_2$ phase studied lie along the tie line that connects the original L64/*o*-xylene solution containing 34.5% w/w L64 with the point that represents 100% water. The binary $L_2$ system investigated contains 86.1% w/w L64 ($Z_w = 1$) and no *o*-xylene.

**ESR Experiments.** ESR spectra were measured with a Bruker X-band spectrometer, Model ECS 106, equipped with the ESP 3240 software system for data acquisition and manipulation and with an ER4111 VT variable temperature unit. Typical conditions for spectra acquisition were as follows: microwave power 2 mW; 100 kHz modulation with widths of 0.2−0.5 G depending on the line width; time constant 10−40 ms; 2k points; 5−10 scans. Spectra were exported from the Bruker data system to ASCII files and plotted with the SpectraCalc software (Galactic Industries Corporation, Salem, NH).

## Results

**ESR Spectra of CAT*n* Spin Probes.** The $L_2$ region of the phase diagram for the L64/$^2H_2O$/*p*-xylene system is presented in Figure 1.[24] The compositions of the *ternary* L64/water/*o*-xylene solutions studied are along the tie line that connects the original L64/*o*-xylene mixture (34.5% w/w L64; indicated by an arrow in Figure 1) with the corner that represents 100% water. The composition of the *binary* L64/water mixture (86.1% w/w L64) in the $L_2$ phase is also shown in Figure 1. ESR spectra were measured for the CAT*n* spin probes series with $n = 1$, 4, 8, 11, and 16 as a function of $Z_w$. Most spectra were measured at 295 K.

Representative spectra at 295 K for the ternary solutions are given in Figure 2A−E, for $Z_w$ in the range 0−2.00. CAT1 is insoluble in the initial L64/*o*-xylene solution ($Z_w = 0$); for $Z_w = 0.25$ the ESR spectrum for CAT1 (Figure 2A, top spectrum) has a sloping baseline, which suggests an additional component with broad signals, most likely due to aggregation of the spin probe in the small polar core. The other spin probes are soluble in the L64/*o*-xylene solution even in the absence of water ($Z_w = 0$). The spectra of CAT4, CAT8, and CAT11 in L64/xylene ($Z_w = 0$) are identical, suggesting that the spectral differences detected in parts A−E are due to the self-assembling of the polymer chains in the

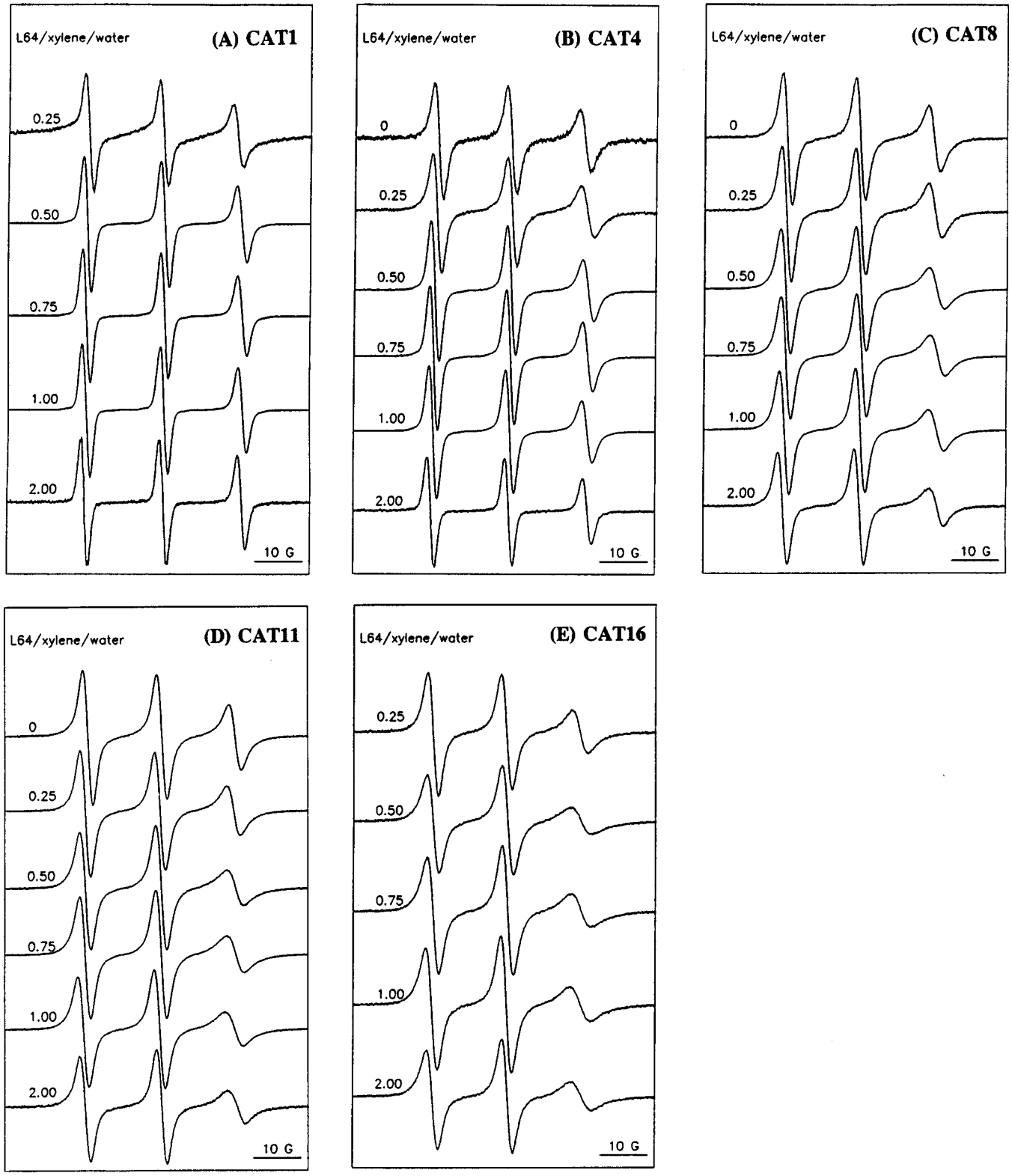


**Figure 2.** Selected X-band ESR spectra at 295 K of CAT*n* spin probes in L64/water/*o*-xylene, as a function of $Z_w$, the number of water molecules per EO unit: (A) CAT1, (B) CAT4, (C) CAT8, (D) CAT11, and (E) CAT16.

presence of water. Two main conclusions can be deduced from the spectra given in Figure 2: **First**, all spectra are of the motionally narrowed type, but differ in their line shape pattern. The line shapes for CAT1 and CAT4 are similar and consist of three lines with decreasing amplitudes (and increasing line widths) with increasing magnetic field. The line shapes for the other probes are similar to those for CAT1 and CAT4 at low water contents, but change to a different pattern, with the center line having the largest amplitude, at higher water contents; the $Z_w$ values corresponding to the change in the line shapes are $\approx$1.00 for CAT8 and only 0.5 for both CAT11 and CAT16. **Second**, the line widths for CAT1 and CAT4 decrease with increasing water content, and proton hyperfine splittings (HFS) can be detected for these probes at $Z_w = 2.00$. For the other probes, the line widths increase with increasing water content.

The spectra of the CAT*n* spin probes are not affected by the oil-soluble paramagnetic $CuX_2$, not even the most

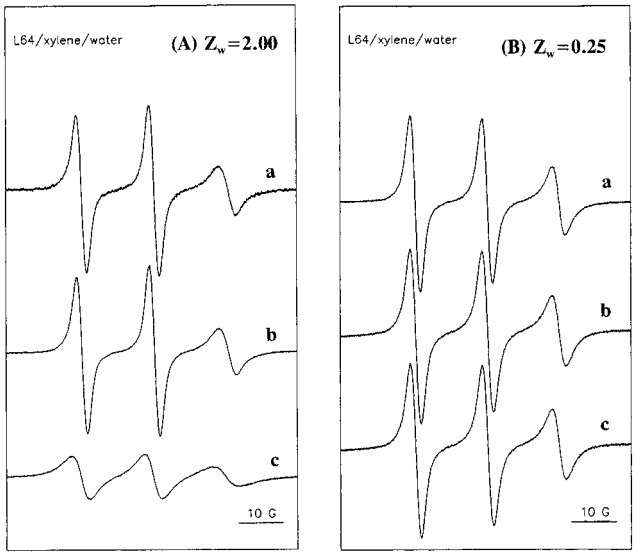


**Figure 3.** Quenching experiments for CAT11 in L64/water/*o*-xylene for two hydration levels: $Z_w = 2.00$ (A) and $Z_w = 0.25$ (B). Spectra in parts A and B represent the original spectrum (**a**), and the spectra obtained by addition of $CuX_2$ (**b**) and of $CuCl_2$ (**c**) at the two $Z_w$ levels.

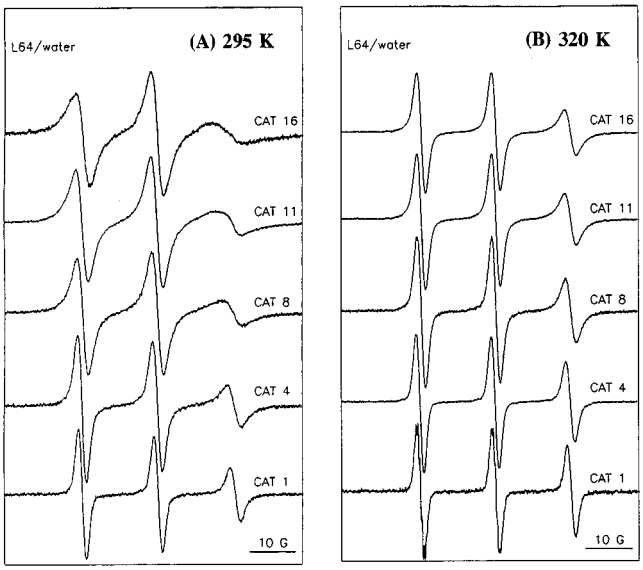


**Figure 4.** X-Band ESR spectra of CAT*n* spin probes in the binary system containing 86.1% w/w ($Z_w = 1$) at 295 K (A) and 320 K (B).

hydrophobic probe CAT16. The effect of $CuCl_2$, however, depends on the water content and is presented in Figure 3. For $Z_w = 2$, Figure 3A, no effect is seen on addition of $CuX_2$ (spectrum **b**) compared to the original spectrum **a**; but the signals are significantly broadened on addition of $CuCl_2$ (spectrum **c**), suggesting that the probe resides in a water environment. For $Z_w = 0.25$, Figure 3B, no effect is seen for addition of either $CuX_2$ or $CuCl_2$; as the probe is clearly in a polar environment, this result suggests that the degree of hydration at the site of CAT11 is very low for $Z_w = 0.25$ and too low to dissolve the $CuCl_2$.

ESR spectra at 295 K of the CAT*n* spin probes ($n$ = 1, 4, 8, 11, and 16) in the binary $L_2$ composition L64/water (86.1% w/w L64, $Z_w = 1$) are shown in Figure 4A. The evolution of the line shapes is similar to that observed for the ternary $L_2$ composition; in addition, the line shapes for the probes with higher $n$ values are broad, and clearly at the threshold of motional averaging. The remaining anisotropic interactions are averaged and the lines are narrower at higher temperature, as seen in the corresponding spectra measured at 320 K, Figure 4B.

**Table 1. Isotropic $^{14}N$ Hyperfine Splittings, $a_N$ (G), of CAT*n* Probes in Reverse Micelles of L64/*o*-Xylene/Water and L64/Water as a Function of $Z_w = [H_2O]/[EO]$**

| | $a_N$ (G) | | | | |
|---|---|---|---|---|---|
| $Z_w$ | CAT1 | CAT4 | CAT8 | CAT11 | CAT16 |
| L64 (34.5% w/w)/*o*-xylene/water, 295 K | | | | | |
| 0 | *a* | 15.45 | 15.45 | 15.45 | ND |
| 0.25 | *b* | 15.90 | 15.70 | 15.50 | 15.40 |
| 0.50 | 16.26 | 16.16 | 15.80 | 15.70 | 15.65 |
| 0.75 | 16.30 | 16.20 | 15.90 | 15.80 | 15.65 |
| 1.00 | 16.40 | 16.25 | 15.90 | 15.80 | 15.65 |
| 2.00 | 16.50 | 16.45 | 16.10 | 15.80 | 15.80 |
| L64 (86.1% w/w)/water, 295 K | | | | | |
| 1.00 | 16.20 | 16.09 | 15.90 | *c* | *c* |
| L64 (86.1% w/w)/water, 320 K | | | | | |
| 1.00 | 16.08 | 16.00 | 15.95 | 15.90 | 15.80 |

[a] Insoluble. [b] See text. [c] Slow motional spectra; ND = not determined. The $a_N$ values for CAT4 are 16.75 G in water at 320 K, 15.65 G in neat PEO (Carbowax 300) at 320 K, 15.34 G in neat PPO at 320 K, 15.33 G in TEGDME at 320 K, and 15.30 G in *o*-xylene at 300 K.

The isotropic $^{14}N$ hyperfine splitting $a_N$ of the CAT*n* probes in the ternary $L_2$ (Table 1) generally increases with water content, but the increase is small for CAT1 (between 16.26 and 16.50 G), and for CAT16 (between 15.4 and 15.8 G); for the same water content, $a_N$ decreases gradually from CAT1 to CAT16. These observations suggest different locations of the CAT*n* spin probes as a function of the composition of the $L_2$ phase. The $a_N$ values in the binary L64/water $L_2$ phase are also given in Table 1; the values for CAT1 and CAT4 are slightly lower than, and that of CAT8 is identical to, the values measured in the ternary $L_2$ phase for the same $Z_w$ value.

**ESR Spectra of *x*DSA Spin Probes.** The *x*DSA spin probes are soluble in *o*-xylene and the corresponding spectra are typical of fast motional averaging, with three lines of similar amplitude. The effect of the reverse micelle formation on the spectrum of the 5DSA spin probe at 295 K is shown in Figure 5A: spectrum **a** is 5DSA/*o*-xylene, spectrum **b** is 5DSA/L64/*o*-xylene, and **c** and **d** are 5DSA spectra in the ternary $L_2$ phase with $Z_w = 0.25$ (in **c**), and $Z_w = 2.0$ (in **d**). The line shapes of 5DSA in the $L_2$ phase with the smaller amount of water, spectrum **c**, are only slightly different compared to the spectra in the absence of water (spectra **a** and **b**), but the spectrum changes dramatically for $Z_w = 2$, where the anisotropic interactions are clearly detected (spectrum **d**). Typical ESR spectra at 295 K in the ternary L64/water/*o*-xylene mixture at high water content ($Z_w = 2$) for the four *x*DSA probes are shown in Figure 5B; predominantly slow-motional type spectra are observed for 5-, 7- and 10DSA, and a motionally narrowed triplet for 16DSA. The spectrum for 7DSA is more complex and suggests an additional component, probably of the fast motional type, indicated by the arrow in Figure 5B. For $Z_w = 1$ the ESR spectra of 5DSA and 7DSA (not shown) consist of two components, slow- and fast motional, respectively, while the ESR spectra of the higher homologs in the series consist of the fast motional component only. The amplitude of the motionally narrowed component in the spectra of the *x*DSA probes can be decreased by addition of the oil-soluble $CuX_2$ paramagnet, as seen in Figure 5C; the

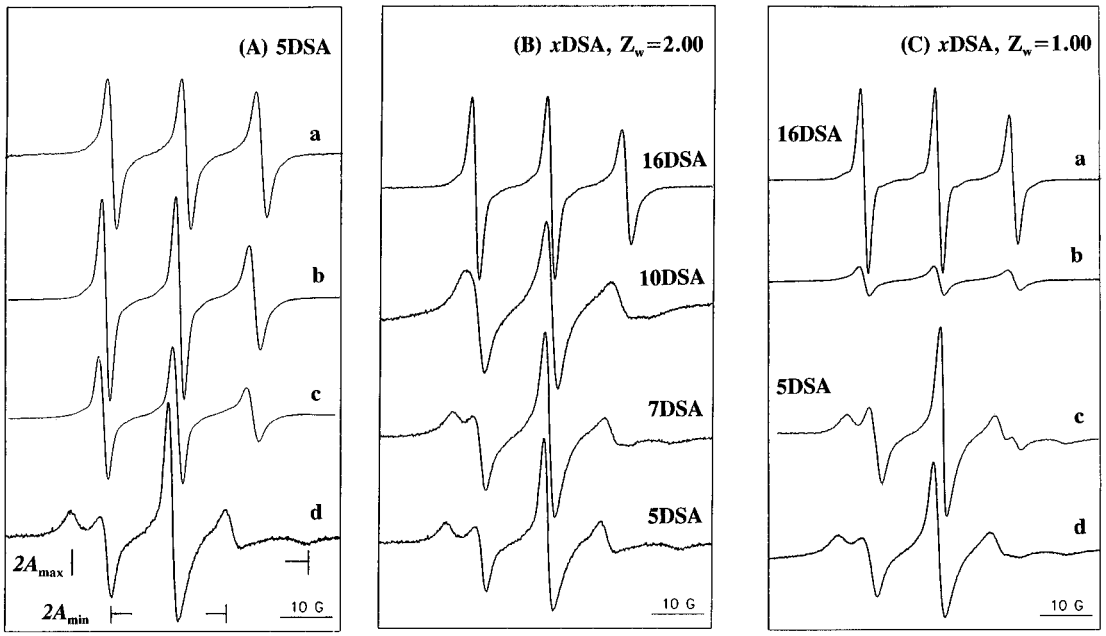


**Figure 5.** (A) X-Band ESR spectra of 5DSA at 295 K in *o*-xylene (**a**), in L64/*o*-xylene (**b**), in L64/*o*-xylene/water with $Z_w = 0.5$ (**c**), and in L64/*o*-xylene/water with $Z_w = 2.0$ (**d**). The $2A_{max}$ and $2A_{min}$ values are shown in spectrum **d**. (B) X-Band ESR spectra at 295 K of *x*DSA spin probes in L64/water/*o*-xylene ($Z_w = 2$). The arrow indicates one of the three lines of the motionally narrowed component in the spectrum of 7DSA. (C) Quenching experiments of *x*DSA spin probes in L64/water/*o*-xylene with $Z_w = 1$. Spectra **a** and **c** are the original ESR spectra for 16DSA and 5DSA, respectively; **b** and **d** are the corresponding spectra after addition of $CuX_2$.

**Table 2. ESR Parameters of *x*DSA Spin Probes in Reverse Micelles of L64 (34.5% w/w)/*o*-Xylene/Water as a Function of $Z_w = [H_2O]/[EO]$**

| $Z_w$ | probe | $a_N$ (G) | $A_{max}$ (G) | $A_{min}$ (G) | *S* |
|---|---|---|---|---|---|
| 0 | 5DSA | 14.3[a] | | | |
| 0.5 | 5DSA | 14.3[a] | | | |
| 1.0 | 5DSA | 14.5[b] | 22.0 | 10.8 | 0.43 |
| 1.0 | 7DSA | 14.3[b] | 20.6 | 11.2 | 0.36 |
| 1.0 | 16DSA | 14.3[a,c] | | | |
| 2.0 | 5DSA | 14.7[b] | 22.4 | 10.9 | 0.43 |
| 2.0 | 7DSA | 14.5[b] | 20.8 | 11.3 | 0.36 |
| 2.0 | 10DSA | 14.0[b] | 17.7 | 12.1 | 0.22 |
| 2.0 | 16DSA | 14.3[a] | | | |

[a] Measured directly. [b] Calculated as $(1/3)(A_{max} + 2A_{min})$. [c] Broadened by $CuX_2$. The $a_N$ of 5DSA in *o*-xylene at 295 K is 14.3 G.

effect of $CuX_2$ addition becomes clear by comparing the original spectra of 16DSA (spectrum **a**) and 5DSA (spectrum **c**) with the corresponding spectra obtained on addition of $CuX_2$, **b** and **d** respectively. The slow motional component is not affected.

The ESR parameters and the order parameter *S* for the *x*DSA spin probes are summarized in Table 2. The $a_N$ values for the slow motional spectral components were calculated from $a_N = (A_{max} + 2A_{min})/3$, and the order parameter *S* from $S = (A_{max} - A_{min})/[A_{zz} - (A_{xx} + A_{yy})/2]$; $A_{max}$ and $A_{min}$ are determined from the experimental spectra,[13] as indicated in Figure 5A. The hyperfine tensor components for the *x*DSA probes determined in lyophilized bovine serum albumin (BSA), $A_{xx} = 6.3$ G, $A_{yy} = 5.8$ g, and $A_{zz} = 33.5$ G,[30] were used and scaled to fit $a_N$, the experimental isotropic $^{14}N$ splitting constant for each probe.[31]

**Effective Hydration.** The $a_N$ values for the CAT*n* series in the ternary $L_2$ compositions are plotted in Figure 6A as a function of $Z_w$, together with the corresponding data for the calibration curve based on CAT4 in aqueous PEO (Carbowax 200).[13] It is clear that the *effective* hydration levels for CAT1 and CAT4 are higher, and that for the larger probe homologs are lower, compared to the *stoichiometric* values $Z_w$ represented by the data for the PEO solution. For CAT11 and CAT16, the $a_N$ values measured for $Z_w = 0.25$ are lower than those measured in pure PEO (see Table 1), suggesting an effect of the less polar PPO environment.

Taking $a_N$ as an index of hydration, the effective degree of hydration $Z_{w,eff}$ at the probe site was deduced by reading on the calibration curve the $Z_w$ value corresponding to the $a_N$ values measured for the probe in the ternary mixture. In this way we obtain Figure 6B, where the effective hydration level $Z_{w,eff}$ is plotted vs $Z_w$ (in the range 0.50−2.00) for all of the probes. $Z_{w,eff}$ represents therefore the real local degree of hydration at the probe site in the aggregated system.

**Dynamics.** Quantitative information on the rate and mechanism of rotation of the spin labels can be obtained by simulating the experimental spectra. Because most of the spectra measured in this study are of the motionally narrowed type, it is difficult to unambiguously determine a set of parameters characterizing the rotational diffusion of the spin label by the simulation process. For this reason we opted for a semiquantitative approach, which involves the analysis of the parameters *A*, *B*, and *C* in the expression for the peak-to-peak line width of each of the three components, $\Delta H(m_I)$, in a motionally narrowed spectrum: $\Delta H(m_I) = A + Bm_I + Cm_I^2$, where $m_I = 1, 0, -1$ is the nuclear spin number corresponding to the low, central, and high field lines, respectively. *B* and *C* can be determined directly from the line heights of the three spectral lines, $h_{+1}$, $h_0$, and $h_{-1}$, respectively, and the peak-to-peak width of the central line, $\Delta H(0)$ in G, using eqs 1 and 2:

$$B = (3^{1/2}/4)\,\Delta H(0)[(h_0/h_{+1})^{1/2} - (h_0/h_{-1})^{1/2}] \quad (1)$$

$$C = (3^{1/2}/4)\,\Delta H(0)[(h_0/h_{+1})^{1/2} + (h_0/h_{-1})^{1/2} - 2] \quad (2)$$

Details on the dynamics will be obtained by comparing the *B* and *C* values determined from the ESR

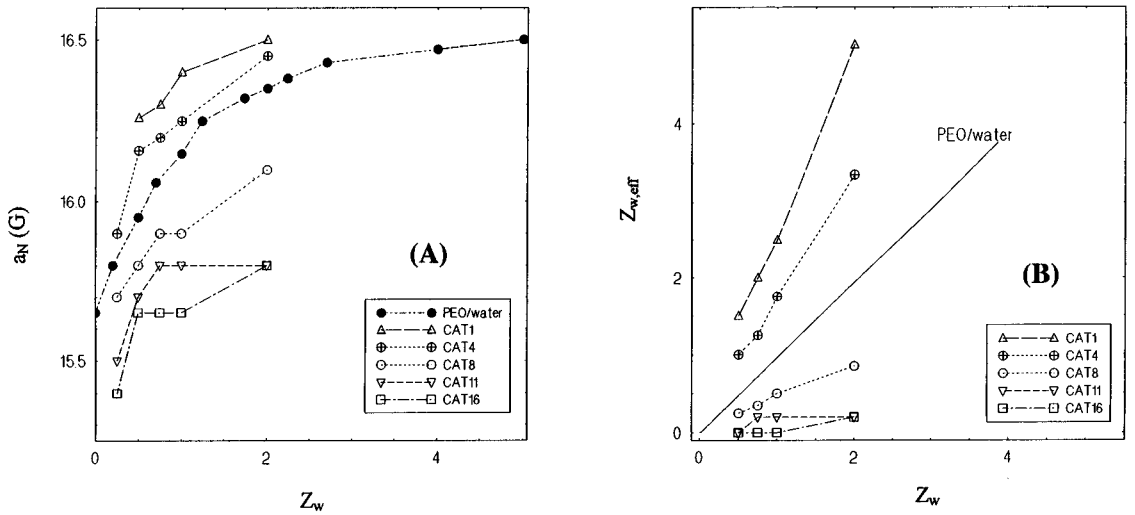


**Figure 6.** (A) Plot of $a_N$ vs $Z_w$ for the CAT*n* series in L64/*o*-xylene/water and for CAT4 in PEO (MW 200).[13] (B) Effective degree of hydration $Z_{w,eff}$ obtained from the $a_N$ values for each probe by reading the $Z_w$ value from the calibration curve, vs the $Z_w$ value in the sample (see text).

spectra with theoretical values that depend on the rotational parameters of the spin labels and their magnetic parameters and can be calculated using eq 5 in the paper of Goldman et al.[32]

The $a_N$ variation with the effective hydration described above implies a dependence of the magnetic parameters of the spin probe on the hydration at the spin probe site. In order to exclude the effect of the different local polarities of the spin probes on the experimental $B$ and $C$ values, we "normalized" the $B$ and $C$ deduced from eqs 1 and 2 to the magnetic parameters for the CAT1 probe in pure water by multiplying the right hand sides of eqs 1 and 2 by $a_{iso}/a_N$ and $(a_{iso}/a_N)^2$, respectively; $a_{iso}$ is obtained from the hyperfine tensor components of CAT1 in water: $A_{xx} = 6.2$ G, $A_{yy} = 7.3$ G, $A_{zz} = 36.2$ G (and $a_{iso} = 16.88$ G), $g_{xx} = 2.0097$, $g_{yy} = 2.0063$, and $g_{zz} = 2.0035$.[33] In this way we obtained the $B_{expt}$ (G) and $C_{expt}$ (G) parameters, which express the dynamics and are not affected by the local polarity reflected in the $a_N$ values for the probes in the different systems. The additional corrections for the unresolved hyperfine splittings were not performed because they are not expected to significantly affect the slope of $B$ vs $C$.[34]

The normalized values $B_{expt}$ (G) vs $C_{expt}$ (G) for the CAT*n* series in the L64 system and for CAT8, CAT11, and CAT16 in Carbowax 300 are plotted in Figure 7, where the absolute values of $B_{expt}$ (G) are plotted.[35,36] We notice that the data for CAT1, CAT4 and for the probes in Carbowax 300 appear to belong to one set (set 1), and the data for the higher spin probe homologs (CAT8, CAT11, CAT16) belong to a different set (set 2), suggesting different motional mechanisms for the two groups of systems.

In order to obtain more details on the motional mechanism, we calculated theoretical values $B_{calc}$ and $C_{calc}$ for various orientations of the rotational tensor symmetry axis, using the axially symmetric rotational diffusion model[37] and the components of the **g** and $^{14}$**N** hyperfine tensor components for CAT1 in pure water.[33] The orientation of the rotational tensor symmetry axis and the degree of anisotropy $N$ ($N = R_{||}/R_{\perp}$, where $R_{||}$ and $R_{\perp}$ are respectively the components of the axially symmetric rotational tensor) were used as parameters. The results of the calculations are presented in Figure 8, where the circles represent $B_{calc}$ and $C_{calc}$ pairs calculated for $\tau_{\perp} = 1 \times 10^{-9}$ s.

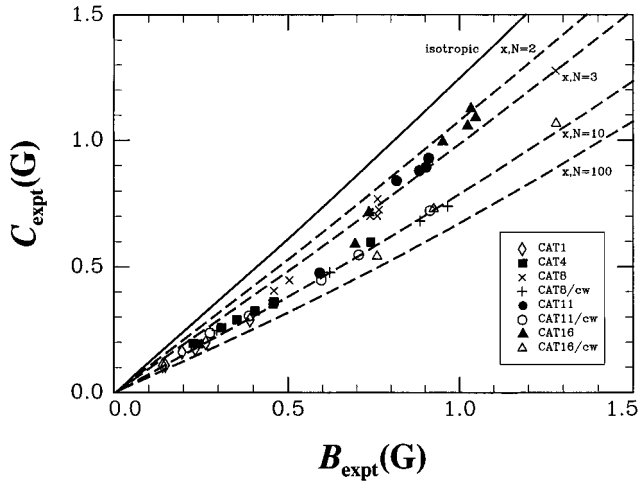


**Figure 7.** Plot of the normalized experimental parameters $C_{expt}$ (G) vs $B_{expt}$ (G) determined from the ESR spectra of the CAT*n* spin probes in the binary and ternary $L_2$ phases and in Carbowax 300 (cw). The calculated $C_{calc}$ vs $B_{calc}$ plots from Figure 8, for rotation about the $x$ axis with $N = 2$, 3, 10 and 100 (- - -) and for isotropic motion (—), are superimposed on the experimental values.

## Discussion

The data presented above suggest in general terms that the probes intercalate in the polymeric aggregates, but different probes choose different sites and report on the local polarity, hydration, and dynamics via the line shapes, the $a_N$ values as a function of the water content, and the type of dynamics. In this section we will correlate the spectral parameters with the probe site, with the structure and dynamics of the micellar assembly and with the onset of micellization.

**Location of CAT*n* Probes and Polarity Profile.** In typical reverse micelles formed by ionic surfactants such as AOT, a water pool is formed, and its size depends on the water content. The polarity profile in the assembled surfactant molecules is a result of the electrical charges of the polar head. By contrast, in the nonionic Pluronic surfactants, the polarity differences are due to the distribution of the water and the organic solvent in the PEO and PPO segments. For simplicity,

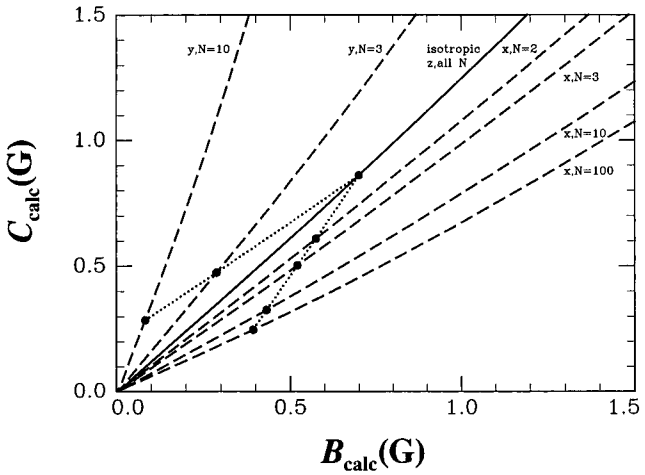


**Figure 8.** Plot of the calculated parameters $C_{calc}$ vs $B_{calc}$ for rotations about the *x*, *y*, and *z* axes with the anisotropy *N* as a parameter and $a_{iso} = 16.88$ G. The circles represent $B_{calc}$ and $C_{calc}$ pairs calculated for $\tau_\perp = 1 \times 10^{-9}$ s.

our model considers the reverse micelles as consisting of two different regions: the hydrophilic core consisting of PEO and water and the hydrophobic corona where the PPO chains are solvated by the organic solvent. Consistent with this model, the variations of $a_N$ in the polar core will be correlated with the local degree of hydration. This approach will not prevent us from noticing experimental evidence that will provide additional refinement of, or even departure from, this model.

In the reverse micelles of AOT/water/isooctane at ambient temperature, the $a_N$ value of CAT16 is 16.5 G, close to that measured in pure water (16.88 G).[3] The data presented in Table 1 indicate that the high $a_N$ value, 16.5 G, is reached only by CAT*1*, at the highest water content, $Z_w = 2$. The $a_N$ values for CAT1 at lower $Z_w$ values, and for the other CAT*n* probes at all $Z_w$ values, are lower than 16.5 G, and vary with the length of the alkyl group (from $n = 1$ to $n = 16$), and with the water content. The general trend is as follows: $a_N$ is lower for lower $Z_w$ values and for an increasing length of the alkyl group. The expectation of a hydrated site for the CAT*n* spin probes series can be reconciled with the different $a_N$ values by assuming that the hydrated region extends over the entire length of the PEO block, and that this region exhibits a hydration *gradient*. The lower $a_N$ values for the higher CAT*n* homologs can be explained by assuming that the hydration level along the PEO segment is lower at sites occupied by these members in the series. We will examine now the data for a given spin probe as a function of $Z_w$ and for the entire set of CAT*n* spin probes at a given $Z_w$ value.

The data for CAT1 are particularly illuminating, because the probe is insoluble in the binary mixture L64/*o*-xylene (in the absence of water). We suggest that the $a_N$ value for the largest amount of water ($Z_w = 2$) is lower than the value in pure water due to a less polar and less hydrated site in the core of the reverse micelles. This suggestion is supported by our study of the L64/water binary system across the phase diagram (as a function of L64 content) using a water soluble but not ionic spin probe, where we have observed a similar behavior.[26] In the reverse micelles of the AOT system,[3] an $a_N$ value for CAT16 lower than that in pure water was justified by assuming a rapid exchange between a water site and a less hydrated site in the interior of the reverse micelles. Examination of the data for CAT1 measured in this study reveals some inconsistencies with the exchange model: in the ternary $L_2$ composition with $Z_w = 1$, $a_N$ is 16.40 G; in the binary $L_2$ mixture, $a_N$ is significantly lower, only 16.20 G. This difference cannot be explained on the basis of the two-site exchange model, which would imply the existence of sites with little or no hydration in the core of the reverse micelles. The line shapes shown in parts A and B of Figure 4 have visible proton hyperfine splitting for CAT1, an effect that would be smeared by exchange between two sites. For all these reasons, we propose that the $a_N$ values for CAT1 and CAT4 represent *local* averages typical of the probe location. The increase of $a_N$ for CAT1 from 16.26 G for $Z_w = 0.50$ (and $Z_{w,eff} \approx 1.2$) to 16.50 G for $Z_w = 2.00$ (and $Z_{w,eff} \approx 5$) is due to increasing hydration of the reverse micellar core. These conclusions complement the results deduced by light scattering, which have suggested a large increase in the size of the reverse micelles for $Z_w > 1.4$, from 90 Å at $Z_w = 1.4$ to 200 Å at $Z_w = 2.5$, due to the increase in the hydrated regions.[22,23]

For a given value of $Z_w$, $a_N$ decreases gradually with increasing size of the probe from $n = 1$ to $n = 16$. Because the higher probes are soluble in *o*-xylene, these values could be interpreted in terms of an exchange between water and "oil" sites. The quenching experiments, however, suggest that the probes are not accessible to the oil-soluble paramagnet $CuX_2$. The unescapable conclusion is therefore that even the higher homologs are in the hydrated regions, and the different $a_N$ values for the different probes suggest different hydration levels along the hydrated EO core. The $a_N$ value for the higher CAT*n* homologs, CAT11 and CAT16, vary little with the water content, suggesting that the local hydration is low and does not increase significantly with the increase of the hydrated core when the amount of water in the system increases. We propose that this is due to anchoring of the alkyl groups in the more hydrophobic PPO domains, so that the cation of the spin probes is very close to the core/corona interface. In support of this idea we note that the $a_N$ value for CAT16 for low $Z_w$ values is close to that in pure PPO. The nitroxide groups of the CAT*n* probes therefore report on the entire core, from the high hydration level sensed by CAT1 to the very low hydration level for CAT16, which is located at the PEO/PPO interface.

An estimate of the scale of the hydration gradient can be obtained by observing that the length of the PEO segment is expected to be ≈48 Å for the planar zigzag, 36 Å for a helical structure, and 27 Å for a random coil.[24] The polarity and hydration of the core in the reversed micelles is therefore explored by the CAT*n* probes on a scale of ≤48 Å.

On the basis of this discussion, we present in Figure 9 the suggested locations of the CAT*n* probes in the core of the reverse micelles: CAT1 and CAT4 near the center of the core, CAT11 and CAT16 near the core/corona interface, and CAT8 at an intermediate position.

**Location of *x*DSA Probes.** The data for the doxyl probes given in Table 2 suggest two conclusions. **First**, the $a_N$ values for these probes for $Z_w = 0-2.00$ are in the range 14.0−14.7 G; some of these values are measured indirectly, from the $A_{max}$ and $A_{min}$ values, and the precision in the determination of $a_N$ is only ±0.3 G. The $a_N$ values of 5DSA for $Z_w = 0$ and $Z_w = 0.5$, measured directly from the spectra, are 14.3 ± 0.05 G, identical to the value of 5DSA in pure *o*-xylene. This

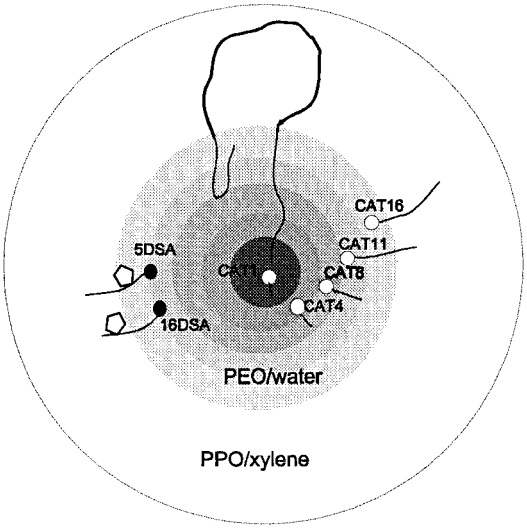


**Figure 9.** Suggested locations for the CAT*n* and *x*DSA spin probes in the reverse micellar aggregates (see text).

behavior can be rationalized by assuming no penetration of water in the PPO regions and anchoring of all *x*DSA probe heads at the PEO/PPO interface, so that the nitroxide groups in the various *x*DSA probes are exploring the corona at different depths. **Second**, the evolution of the ESR spectra presented in Figure 5, from the slow motional type for 5DSA to motionally averaged for 16DSA, reflects the gradient of *order* in the corona, on a scale of ≤24 Å, which is the length of the fully extended DSA group.[25] The order parameter deduced from the spectra does not seem to change significantly as a function of water content for $Z_w > 1$, as expected for the location of the *x*DSA probes suggested above. More data, such as temperature variation of the ESR spectra and simulations, are needed to fully explore the potential information from these amphiphilic probes. At this stage, we note that the use of solutions of the surfactant in 0.1 M NaOH rather than water facilitates the interpretation of the data, and enables an unambiguous determination of the location of the *x*DSA probes.

On the basis of the two conclusions mentioned above, we added in Figure 9 the suggested positions of these probes in the *o*-xylene-rich PPO corona. The CAT*n* and *x*DSA spin probes are located therefore on the hydrophilic (PEO) and hydrophobic (PPO) side, respectively, of the interface between the core and the corona in the reverse micelles based on L64. In Figure 9 we have indicated a bent conformation for the triblock; the justification for this structure is in the lack of "gelation", or dramatic increase in viscosity of the solution expected for a conformation that would provide connectivity between various reverse micelles.

The discussion on the location of the probes emphasizes the different type of information that can be obtained from spin probes that differ in size, structure, and polarity.

**The Micellization Process.** In the ternary $L_2$ region for $Z_w = 0$, the CAT*n* spin probes with $n = 4$, 8, and 11 have identical $a_N$ values, 15.45 G, a value between that in *o*-xylene (15.36 G) and that in pure PEO (15.65 G). The fact that probes with different hydrophobicities have the same $a_N$ value is an indication that there are no possibilities for different locations for the ionic head groups, because the polar region is very small. In the ternary $L_2$ region for $Z_w = 0.25$, the CAT*n* spin probes with $n = 4$, 8, 11, and 16 have the same spectral pattern (decreasing amplitude with increasing magnetic field) and decreasing $a_N$ values. The tumbling rates of the long-tail probes is slower, as seen by comparing the relative heights of the signals for one probe, and the line widths of the different probes for a given $m_I$ value (Figure 2B−E). The hindrance to rotation increases with the length of the tail. These facts suggest the emergence of a micellar microphase with sites of various polarity, and constraints on the probe mobility in the hydrated region: the onset of micellization. However, the hydrated regions are not extensive, and $CuCl_2$ fails to reach and broaden the lines of CAT11, located in a low hydration region, as seen in Figure 3.

At $Z_w = 0.5$, a complete polarity profile develops, with different $a_N$ values for each probe, from 16.26 G for CAT1 to 15.60 G for CAT16. With further increase in water content, the polarity of the core increases continuously, more rapidly in the center compared to the periphery, as seen from the data given in Table 1. The values of $Z_{w,eff}$ (Figure 6) suggest that CAT1 and CAT4 experience higher than average hydration ($Z_w = 2$ and $Z_{w,eff} = 4$, and $Z_w = 1$ and $Z_{w,eff} = 2.5$ for CAT1) and CAT8 and CAT11 experience lower than average hydration ($Z_w = 2$, $Z_{w,eff} \approx 1$ for CAT8), while at the CAT16 site there is practically no hydration.

In previous studies of reverse micelles in nonionic surfactants it has been found that the chemical nature of the organic solvent has a considerable influence on the polar core. For example, the water segregation was considerably more pronounced for $C_{12}E_4$ in cyclohexane, compared to decane.[9] The phase diagram of the binary L64/water system indicates a considerable $L_2$ phase in the polymer-rich region.[38] This spin probe study was undertaken to obtain evidence for self-assembling and for the formation of the reverse micelles. While in a mixture that is homogeneous on the *molecular* level all CAT*n* probes are expected to have nearly identical $a_N$ values, as was observed for these probes in Carbowax/water mixtures, a polarity profile is expected in organized systems. Therefore the ESR spectra of the CAT*n* series represent a valuable test for the appearance of the reverse micelles. The concentration of L64 was selected to correspond to $Z_w = 1$, in order to facilitate the comparison with the $L_2$ phase in the ternary system. At higher $Z_w$ values, for instance for $Z_w = 2$, the binary system changes to the lamellar phase,[38] because as the polar head increases, the curvature decreases.[21] In contrast, the reverse micelles in the ternary system are stable at $Z_w = 2$, because the hydrophobic part is larger due to the solvation by *o*-xylene; and the condition for the formation of the lamellar phase is reached at a higher degree of hydration.[24]

The data presented in Table 1 for the binary L64/water system confirm the existence of water-rich domains, with a polarity profile. Compared to the ternary RM system with the same water content, the segregation of water is less pronounced: the highest effective hydration value, as measured by CAT1, is $Z_{w,eff} = 1.2$ for $Z_w = 1$, compared to $Z_{w,eff} = 2.5$ in the ternary system. The value for CAT4 ($Z_{w,eff} = 0.8$) falls below the *average* water content. CAT8 reflects an environment similar to that in the ternary system. Unfortunately, it was impossible to determine accurately the $a_N$ values for CAT11 and CAT16 at 295 K in the binary system, because the spectra are outside the motional narrowing regime (Figure 4A), an indication of the much

higher viscosity in the absence of the organic solvent. However, the trends of $a_N$ at 320 K (Figure 4B) suggest that the hydration in the outer regions of the core is not decreased. All data for the binary composition suggest therefore the formation of reverse micelles with a polarity profile in the binary $L_2$ system L64/water that is more gradual and less steep, compared to the ternary system.

**Motional Mechanism.** Comparison of the $B_{expt}$ and $C_{expt}$ values deduced from the spectra (Figure 7) with the calculated values (Figure 8) enables the determination of the motional mechanism predominant in the systems represented by sets 1 and 2 above. For clarity, the calculated values for rotation about $x$ with $N = 2$, 3, 10, and 100 as well as for isotropic motion are superimposed on the experimental data in Figure 7. In the assignment of the axis of rotation, we excluded rotations with the symmetry axis oriented along the nitroxide $z$ axis, for steric reasons; in addition, rotations about $y$ are clearly incompatible with the experimental results, as seen in Figure 8. Comparison of the experimental and calculated $C$ vs $B$ dependence indicates excellent agreement for rotation about the N−O bond ($x$ axis), with $N = 10$ for set 1 (including all data for the CAT$n$ probes in Carbowax 300), and $N = 2-3$ for set 2. This result suggests that in the systems represented by set 1, the spin probes are oriented due to the interactions between the cationic charge and the water dipoles, and the motional anisotropy is high. The less anisotropic rotational motion for the probes represented in set 2 suggests that the dominant interactions are between the alkyl chain and the organic solvent in the less polar PPO regions, leading to a more compact, spherical, conformation of the larger probes. In support of this picture we notice that the data for the largest probe, CAT16, are best represented by the lowest anisotropy, $N = 2$. The different dynamics for set 2 is most likely due to the lower local degree of hydration and thus provides additional support for the model of the gradient of the hydration in the core of the reverse micelles. Another way of looking at the nearly isotropic motion for set 2 is to consider that the motion is highly hindered by the alkyl tail, and motions in all directions are significantly reduced. The different rotational mechanism for the two sets of data is clearly determined by the different probe sites, and is consistent with the locations of the CAT$n$ probes suggested in Figure 9.

## Conclusions

The $L_2$ (reverse micellar) phase of $EO_{13}PO_{30}EO_{13}$ (Pluronic L64), was studied in the ternary mixture L64/water/*o*-xylene and in the binary mixture L64/water, using the nitroxide spin probe ESR method. The spin probes differed in size, structure, and polarity and belong to two main types: cationic probes (CAT$n$) with $n$, the number of carbon atoms in the alkyl substituent, equal to 1, 4, 8, 11, and 16; amphiphilic probes based on $x$-doxyl stearic acid ($x$DSA) with $x$, the carbon atom to which the doxyl group is attached, equal to 5, 7, 10, and 16.

The gradient of hydration in the PEO core was deduced on a scale of ≤48 Å from the analysis of $a_N$, the isotropic hyperfine splitting of $^{14}N$ in the CAT$n$ series. The lower homologs in the series ($n = 1$, 4) are located near the center of the hydrated core, while the higher homologs ($n = 11$, 16) are located at the interface between the hydrated core and the *o*-xylene-swollen PPO regions. CAT8 seems to be at an intermediate location. The effective hydration $Z_{w,eff}$ and the hydration gradient were estimated by comparison with a "calibration curve" based on CAT4 in aqueous solutions of PEO, where no self-assembling is expected.

The $x$DSA probes have their head group at the interface between the core and the PPO regions, but the nitroxide groups are in the PPO regions and report on the degree of order in these regions. No evidence for the penetration of water in the PPO regions was obtained in this study.

The dynamics of the CAT$n$ probes reflects the local environment: the motional mechanism of the lower homologs in the series is primarily a rotation around the N−O bond ($x$ axis) with $N = 10$; in contrast, the rotational motion of the higher homologs is close to isotropic, $N = 2$. This difference is due to the probe sites and provides additional support for the location of the probes deduced in this study.

**Acknowledgment.** This study was supported by the Polymers Program of the National Science Foundation, and the Grant Agency of the Academy of Sciences of the Czech Republic (Grant No. 450416). The stay in Detroit of A.C. was supported by the National Research Council Collaboration in Basic Science and Engineering (COBASE) between the United States and Romania. The authors are grateful to Professor B. Bales (California State University, Northridge, CA) for an illuminating discussion. S.S. is grateful to Professor Isao Ando and his group at the Tokyo Institute of Technology for their warm hospitality during her sabbatical stay in Tokyo, where this paper was completed.

## References and Notes

(1) *Reverse Micelles*; Luisi, P. L., Straub, B. E., Eds.; Plenum Press: New York, 1984.
(2) *Structure and Reactivity in Reverse Micelles*; Pileni, M. P., Ed.; Elsevier: Amsterdam, 1989.
(3) Haering, G.; Luisi, P. L.; Hauser, H. *J. Phys. Chem.* **1988**, *92*, 3574.
(4) Lossia, S. A.; Flore, S. G.; Nimmala, S.; Li, H.; Schlick, S. *J. Phys. Chem.* **1992**, *96*, 6071.
(5) Okazaki, M.; Toriyama, K. *J. Magn. Reson.* **1988**, *79*, 158.
(6) Ravey, J. C.; Buzier, M.; Picot, J. C. *J. Colloid Interface Sci.* **1984**, *97*, 9.
(7) Ravey, J. C.; Buzier, M.; In *Surfactants in Solution*; Mittal, K. L., Lindman, B., Ed.; Plenum Press: New York, 1985; Vol. 3, p 1759.
(8) Olsson, U.; Würz, U.; Strey, R. *J. Phys. Chem.* **1993**, *97*, 4535.
(9) Friberg, S. E.; Christenson, H.; Bertrand, G.; Larsen, D. W. In *Reverse Micelles*; Luisi, P. L., Straub, B. E., Eds.; Plenum Press: New York, 1984; p 105.
(10) Strey, R. *Colloid Polym. Sci.* **1994**, *272*, 1005.
(11) Zhu, D.-M.; Wu, X.; Schelly, Z. A. *J. Phys. Chem.* **1992**, *96*, 7121 and references therein.
(12) Caldararu, H.; Caragheorgheopol, A.; Dimonie, M.; Donescu, D.; Dragutan, I.; Marinescu, N. *J. Phys. Chem.* **1992**, *96*, 7109.
(13) Caldararu, H.; Caragheorgheopol, A.; Vasilescu, M.; Dragutan, I.; Lemmetyinen, H. *J. Phys. Chem.* **1994**, *98*, 5320.
(14) Almgren, M.; Brown, W.; Hvidt, S. *Colloid Polym. Sci.* **1995**, *273*, 2.
(15) Alexandridis, P.; Hatton, T. A. *Colloids Surf. A* **1995**, *96*, 1.
(16) *Pluronic and Tetronic Surfactants*; Technical Brochure; BASF Corp.: Parsipanny, NJ, 1989.
(17) (a) Karlstrom, G. *J. Chem. Phys.* **1985**, *89*, 4962. (b) Anderson, M.; Karlstrom, G. *J. Chem. Phys.* **1985**, *89*, 4957.
(18) Linse, P. (a) *Macromolecules* **1993**, *26*, 4437; (b) *J. Phys. Chem.* **1993**, *97*, 13896.
(19) Hurter, P. N.; Scheutjens, J. M. H. M.; Hatton, T. A. *Macromolecules* **1993**, *26*, 5030.
(20) Holland, R. J.; Parker, E. J.; Guiney, K.; Zeld, F. R. *J. Phys. Chem.* **1995**, *99*, 11981.
(21) Israelachvili, J. *Intermolecular and Surface Forces*, 2nd. ed.; Academic Press: London, 1991; p 381.
(22) Wu, G.; Zhou, Z.; Chu, B. *Macromolecules* **1993**, *26*, 2117.

(23) Wu, G.; Chu, B.; Schneider, D. K. *J. Phys. Chem.* **1994**, *98*, 12018.
(24) Alexandridis, P.; Olsson, U.; Lindman, B. *Macromolecules* **1995**, *28*, 7700.
(25) Zhou, L.; Schlick, S. *Polym. Prepr. (Am. Chem. Soc., Div. Polym. Chem.)* **1996**, *37*, 829.
(26) Malka, K.; Schlick, S. *Macromolecules* **1997**, *30*, 456.
(27) Szajdzinska-Pietek, E.; Schlick, S.; Plonka, A. *Langmuir* **1994**, *10*, (a) 1101. (b) 2188. (c) Szajdzinska-Pietek, E.; Schlick, S. In *Ionomers: Characterization, Theory and Applications*; Schlick, S., Ed.; CRC Press: Boca Raton, FL, 1996, Chapter 7.
(28) Kutsumizu, S.; Schlick, S. *Polym. Prepr. (Am. Chem. Soc., Div. Polym. Chem.)* **1996**, *37*, 825.
(29) Kutsumizu, S.; Hara, H.; Schlick, S. *Macromolecules*, in press.
(30) Gaffney, B. J. In *Spin Labeling, Theory and Applications*; Berliner, L. J., Ed.; Academic Press: New York, 1976; p 570.
(31) Szajdzinska-Pietek, E.; Pilar, J.; Schlick, S. *J. Phys. Chem.* **1995**, *99*, 313.
(32) Goldman, S. A.; Bruno, G. V.; Polnazsek, C. F.; Freed, J. H. *J. Chem. Phys.* **1972**, *56*, 716.
(33) Ottaviani, M. F.; Baglioni, P.; Martini, G. *J. Phys. Chem.* **1983**, *87*, 3147.
(34) Bales, B. In *Biological Magnetic Resonance*; Berliner, L. J., Reuben, J. Eds.; Plenum Press: New York, 1989; Vol. 8, Chapter 2.
(35) When defining $\Delta H$ in terms of $m_I$ as done in this paper, $B$ is negative. In some cases, for instance in ref 34, $\Delta H$ is defined in terms of the spectral index $M$, and $B$ becomes positive.
(36) Pilar, J.; Labsky, J.; Schlick, S. *J. Phys. Chem.* **1995**, *99*, 12947.
(37) Pilar, J.; Labsky, J. *J. Phys. Chem.* **1984**, *88*, 1984. Equation 2 in this paper was used to obtain $B_{calc}$ and $C_{calc}$.
(38) Zhang, K.; Khan, A. *Macromolecules* **1995**, *28*, 3807.

MA9617328